Catalysis Science & Technology

The Effects of Active Site and Support on Hydrogen Elimination over Transition-Metal-Functionalized Yttria-Decorated Metal–Organic Frameworks

Journal:	*Catalysis Science & Technology*
Manuscript ID	CY-ART-05-2019-001069.R1
Article Type:	Paper
Date Submitted by the Author:	10-Sep-2019
Complete List of Authors:	Yang, Bo; University of Minnesota, Department of Chemistry Sharkas, Kamal; Central Michigan University, Department of Physics Gagliardi, Laura; University of Minnesota, Department of Chemistry and Supercomputing Institute Truhlar, Donald; Department of Chemistry, University of Minnesota

The Effects of Active Site and Support on Hydrogen Elimination over Transition-Metal-Functionalized Yttria-Decorated Metal–Organic Frameworks

Bo Yang, Kamal Sharkas, Laura Gagliardi,* and Donald G. Truhlar**

Department of Chemistry, Inorganometallic Catalyst Design Center, Chemical Theory Center, and Minnesota Supercomputing Institute, University of Minnesota, Minneapolis, Minnesota 55455-0431, USA.

E-mail: yang3227@umn.edu, gagliard@umn.edu, truhlar@umn.edu

KEYWORDS: catalyst design, computational catalyst screening, functionalized metal–organic framework, hydrogen elimination, NU-1000, Sabatier principle, support effect, volcano plot

ABSTRACT: Hydrogen elimination from a metal alkyl complex and its reverse reaction are critical elementary steps in many catalytic cycles. In understanding such catalytic cycles, it is important to learn about the effect of the active site as well as effects beyond the active site, especially support effects. Here we employ density-functional-theory-based computational screening of transition-metal-functionalized yttria-decorated NU-1000 metal–organic frameworks to study the effect of metal sites and supports on the hydrogen elimination reactions. We consider six transition metals. The screening shows that a Nb-based catalyst has the lowest free energy of activation for both α-H elimination and β-H elimination, but for the latter we must also consider the free energy of release of the alkene. By the Sabatier principle, the optimal catalyst for β-H elimination is the one that interacts with molecules with intermediate strength for easy reactant activation as well as easy product desorption. By employing a volcano plot to find the optimum compromise, we identified V-functionalized, yttria-decorated NU-1000 as the most active catalyst among the trial candidates for the β-H elimination reaction. The analysis also reveals a support-specific charge transfer process in which the yttria and carboxylate linkers enable electron transfer between the transition-metal site and organic linkers of the NU-1000 simultaneously with a coordinated change of spin at the metal site and in the linker groups. Based on our analyses, we hypothesize that the observed charge transfer enables certain functional groups, such as propyl, to interact more strongly with the support and stabilize the catalyst.

1. Introduction

Hydrogen elimination from metal alkyl complexes and the reverse reactions are fundamental transformations that occur in both homogeneous and heterogeneous catalysis.[1,2,3,4,5] At least one of these reactions is an elementary step in many catalytic cycles involving olefins, and hydrogen elimination is also a main decomposition pathway of metal alkyls. One finds that α-hydrogen elimination is frequently involved in generating synthetically useful transition-metal alkylidene complexes,[6] and β-hydrogen elimination and the reverse olefin insertion occur in dehydrogenation of alkanes,[7,8,9] Heck-Mizoroki olefination,[10] olefin isomerization,[11] cycloisomerizations,[12] hydroformylation of internal olefins to *n*-aldehydes[13,14] and olefin hydrogenation.

Extensive mechanistic studies have been conducted on hydrogen elimination from transition-metal alkyl complexes.[1,15] These studies have revealed a common reaction pathway that requires an open coordination site, and in the case of β-hydrogen elimination, the pathway is expected to usually involve a four-center cyclic transition state with a coplanar arrangement of the metal, the hydrogen, and two carbon atoms as shown in Figure 1[16]. The α-hydride elimination reaction is an oxidative addition reaction in which a hydride is transferred from the alpha-position of an alkyl ligand to a metal center, thereby generating an alkylidene group and a hydride ligand (when a bis(alkyl) complex is used as the starting material, the hydride can then combine with an alkyl by reductive elimination to generate a new alkane – the result of this two-step process is the same as a one-step alpha-hydride abstraction). The β-hydride elimination produces an olefin hydride complex, which usually generates the final product by desorbing the olefin. In experiments, it is difficult to isolate the hydrogen elimination reaction or specific intermediates,[17] and there is no systematic way to directly study the steric and electronic effects experimentally.[18] Therefore the insight provided by quantum mechanical computations can be an invaluable aid in the understanding of full catalytic cycles as part of the design of new catalysts.

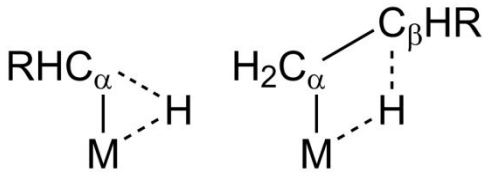

Figure 1. Schematic transition state for (left) α-H elimination and (right) β-H elimination.

Metal–organic frameworks (MOFs), which involve inorganometallic nodes and organic linkers, provide a wide variety of crystalline porous materials with high porosity and large surface area.[19,20,21,22,23,24] Due to their tunable surface structures[25] and their capability for post-synthetic functionalization, MOFs have been widely applied for the anchoring of homogeneous organometallic catalysts. This method, known as surface organometallic chemistry[26,27,28,29,30,31], produces catalysts with high concentrations of active sites.[32,33,34,35] With well-separated nodes and linkers, MOFs also permit a reproducible synthesis of uniform structures with well-defined catalytic sites that are ideal for both full experimental structural characterization and theoretical computations with cluster-based quantum mechanical models.[36]

Here we report computational screening of transition-metal-functionalized yttria-decorated NU-1000 MOFs[37] as catalyst candidates for the hydrogen elimination reaction using Kohn–Sham density functional theory (KS-DFT) to elucidate the effect of metal supports and metal sites. The structures of the screened catalysts are provided in Figure 2. The NU-1000 MOF has the formula $[Zr_6(\mu^3\text{–}O)_4(\mu^3\text{–}OH)_4(OH)_4(OH_2)_4](TBAPy)_2]$, where H_4TBAPy denotes 1,3,6,8-tetrakis(*p*-benzoic-acid)pyrene; it has high chemical and thermal stability under catalytic reaction conditions[38], and its large mesoporous channels facilitate the transport of large molecules.[22,39,40] The zirconium oxide node of the NU-1000 MOF will be called the Zr_6 node, and it serves here as the support for catalyst tethering.

The yttria is introduced between adsorbed transition-metal active sites and NU-1000 nodes. The motivation for including the yttria layer is that it removes the hydroxyl and aqua groups from the NU-1000 node and thus prevents the unwanted hydrogenation reaction between the adsorbed transition-metal active sites and the Zr_6 node. Other tri-valent-metal-based metal oxides such as alumina can provide the same protection for the catalytic center, and the alumina-decorated NU-1000 (Al_2O_2@NU-1000) has been experimentally synthesized by atomic layer deposition in MOFs (AIM)[41]. However, as shown in Figure 3, which compares the alumina layer to the yttria layer, the Al atom tends to have a tetrahedral coordination structure that would result in a longer separation distance between the two O atoms that are used for anchoring transition-metal centers. The long distance between these two O atoms can make it difficult to form transition-metal–O bonds, especially for transition-metals with small covalent radii such as Cr and V. On the other hand, Y atom is more flexible than Al in terms of coordination structure and has a larger covalent radius than other trivalent metals such as In, Ga, Sc or Al. These properties of the Y atom allows easy deposition of the transition-metal centers on top of the yttria layer. Even though the yttria decorated

NU-1000 is yet to be synthesized, the yttria has been deposited experimentally on zirconia through the atomic layer deposition method[42,43].

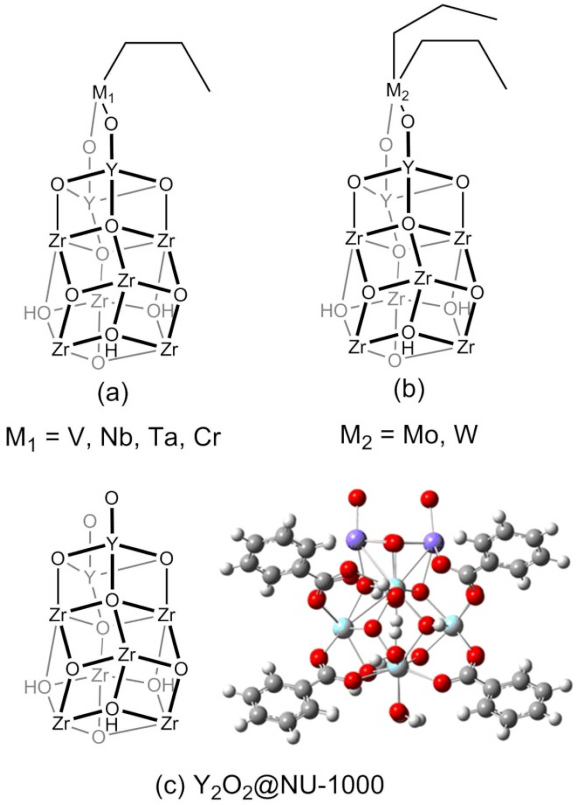

Figure 2. Schematic structures of (a) transition-metal propyl and (b) bis(propyl) complexes deposited on (c) yttria-decorated NU-1000 MOF (Y_2O_2@NU-1000). The formal oxidation state of the transition metal depends on the number of attached propyl ligands. Benzoate groups are used in replacement of the benzoate pyrene linkers of NU-1000 in all of the cluster model calculations reported here, but are removed in the schematic structures shown here for clarity of display. A ball-and-stick model of (c) is given with C atoms shown in grey, H in white, O in red, Zr in cyan, Y in purple.

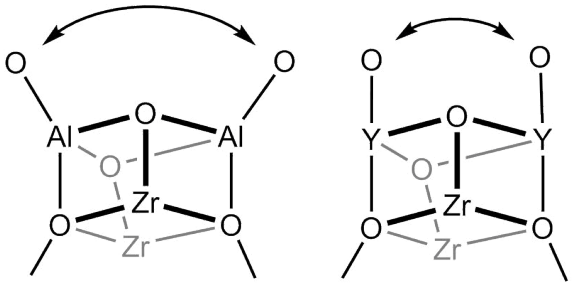

Figure 3. Scheme showing the active site portions of (left) alumina decorated NU-1000 and (right) yttria decorated NU-1000. Part of the NU-1000 node is unshown in each structure to allow better viewing of the structural issue discussed in the text. The

arrows point to the two top O atoms, which are used for anchoring transition-metal centers.

Our mechanistic study illustrates the activity of selected transition-metal candidates for catalysis of the hydrogen elimination processes, and it leads to a volcano plot[44,45] for the identification of active catalysts for the β-H elimination reaction by also considering the product desorption. Charge and spin density analyses are performed to further the understanding of the electronic effect of the yttria-decoration of the NU-1000 MOF on the supported metal alkyl complexes.

2. Computational Methods

All calculations were carried out using KS-DFT by using *Gaussian 09*[46] and *Gaussian 16*[47] software. All species were studied in vacuum using a cluster model for the NU-1000 MOF. The cluster model was created from an optimized periodic unit cell by replacing the benzoate pyrene linkers of NU-1000 with simple benzoates.[48] We then fixed the six carbon atoms of each benzoate ring at their positions in the periodic structure[48] of the MOF; all other atoms were relaxed during geometry optimization. Such cluster model has been shown to accurately describe the catalytic properties of transition-metal complexes attached to the NU-1000 nodes.[25,49]

The 6-31G* basis set[50,51] was chosen for the C, H, O atoms, and the def2-TZVP basis set[52,53] was chosen for the transition-metal ions. We used the M06-L[54] local exchange-correlation functional, which shows high accuracy for transition-metal chemistry.[55,56] Because M06-L is a local functional with no nonlocal Hartree–Fock exchange, but the inclusion of Hartree-Fock exchange in density functionals can affect the spin-state ordering of certain transition-metal complexes,[55,57,58] we tested the effect of Hartree-Fock exchange by also carrying our calculations for some complexes with the hybrid M06[59] functional, which has 27% Hartree-Fock exchange, and we found that for all of the tested complexes, the hybrid M06 functional predicts the same spin-state ordering as the local M06-L functional.

The tested complexes include the Ta- and Nb-based propyl and hydride complexes deposited on Y_2O_2@NU-1000, and Mo-based bis(propyl) and propyl hydride complexes deposited on Y_2O_2@NU-1000. We also verified that the M06 functional gives similar reaction barriers to those obtained with the M06-L functional when used with the same basis sets. For example, the calculated free energy of activation for α-H elimination over Nb catalysts supported on Y_2O_2@NU-1000 is 9.7 kcal/mol using the M06 functional and is 3.9 kcal/mol higher than that obtained using the M06-L functional. In the rest of the paper, all values in the text are obtained by M06-L.

We first optimized the geometries of reagents, transition structures, and reactive intermediates. We calculated geometries for singlet and triplet states of the V, Nb, Ta, Mo, and W systems and for doublet and quartet states of the Cr system. For each case, various starting geometries were considered. Spin contamination is small (the computed expectation value of S^2 has less than a 5% difference from the correct value of $S(S+1)$, where S is half the number of unpaired electrons) in all cases with the exception of Cr-based doublet intermediates where the S^2 expectation value can be as large as 1.02 (36% larger than the correct value of 0.75). Transition structures were optimized using the eigenmode following method by using the *Gaussian* keyword TS. Frequency analysis was performed on all optimized geometries; for each equilibrium geometry, we verified that all frequencies of stable species are real, and for each transition structure we verified that there is only one imaginary frequency.

For each optimized geometry, we computed the enthalpy at 0 K (H_0, equal to the Born-Oppenheimer electronic energy E including nuclear repulsion plus the zero-point vibrational energy), the enthalpy at 298.15 K (H_{298}), and the Gibbs free energy at 298.15 K (G) for a standard partial pressure of 1 atm for each gaseous species. The thermochemical analysis was performed using the quasiharmonic approximation, by which we mean using harmonic oscillator formulas with scaled frequencies[60] to remove systematic errors in electronic structure methods and to provide a simple estimate of high-frequency anharmonic effects on zero-point energies; we used scaling factors of 0.976 to compute the frequencies to obtain H_0, H_{298}, and G. Real frequencies below 100 cm^{-1} are raised to 100 cm^{-1} to simulate low-frequency anharmonic effects.[61] The calculated E, H_0, and H_{298} (Online Resource 1) are given along with the optimized coordinates (Online Resource 2) as the Electronic Supplementary Material (ESM). In the article paper, we only discuss free energies, in particular, free energies of reaction (ΔG) and free energies of activation ($\Delta G^{\ddagger}$), both at 298.15 K.

3. Results and Discussion

3.1 Support effect: Case study of the Ta functionalized, yttria-decorated NU-1000

To understand the support effect of Y_2O_2@NU-1000 on hydrogen elimination catalysis, we compared energies and electron distributions of supported complexes to those of their unsupported analogs. For the unsupported complexes, the structures are constructed by removing the Y_2O_2@NU-1000 node (as defined in Figure 2) and capping the transition-metal with hydroxyl (-OH) groups so that the coordination number of the transition-metal is kept unchanged. Figure 4 shows the structures of the unsupported Ta propyl complex and its analogs on the Y_2O_2@NU-1000 support.

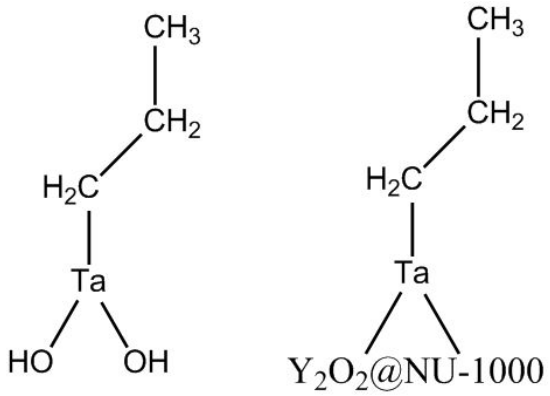

Figure 4. Scheme showing (left) unsupported hydroxylated Ta propyl complex and (right) Ta propyl complex supported on Y_2O_2@NU-1000. The Y_2O_2 @NU-1000 represents the cluster geometry as shown in Figure 2.

3.1.1 Support-induced stabilization of the catalyst

Figure 5 shows free energy profiles for the Y_2O_2@NU-1000-supported system and the unsupported system on singlet and triplet potential energy surfaces (PES), Table 1 summarizes the corresponding free energies for the reactants, products, and transition states.

As shown in Figure 5, as compared to the unsupported system, the Y_2O_2@NU-1000 support increases the free energy of activation for the Ta-complex-catalyzed α-H elimination reaction. When the Ta-based complex is not supported, all of the optimized geometries along the α-H elimination pathway including the propyl (i.e. $Ta(CH_2CH_2CH_3)$), the hydride propylidene (i.e. $Ta(H)(=CHCH_2CH_3)$), and the corresponding transition state (TS) geometry favor the singlet spin configuration rather then the triplet. Accordingly, the α-H elimination over unsupported Ta catalyst prefers to occur on the singlet PES with a free energy of activation of 4.0 kcal/mol and a free energy of reaction of -20.3 kcal/mol.

On the other hand, comparing the Y_2O_2@NU-1000 supported Ta catalyst to its unsupported analogs, we observe the decrease in relative free energies of the triplet intermediates along the reaction path. Specifically, the singlet spin states of the $Ta(CH_2CH_2CH_3)$ and the unsupported TS are favored by free energies of 7.5 and 28.7 kcal/mol, respectively, but the triplet spin states in the corresponding supported cases are favored by 10.4 and 0.8 kcal/mol, respectively. For the $Ta(H)(=CHCH_2CH_3)$ complex, the singlet spin state is favored in both the unsupported system and supported systems, but the free energy difference between the singlet and triplet spin states is decreased from 39.5 kcal/mol in the unsupported system to 15.8 kcal/mol in the supported system.

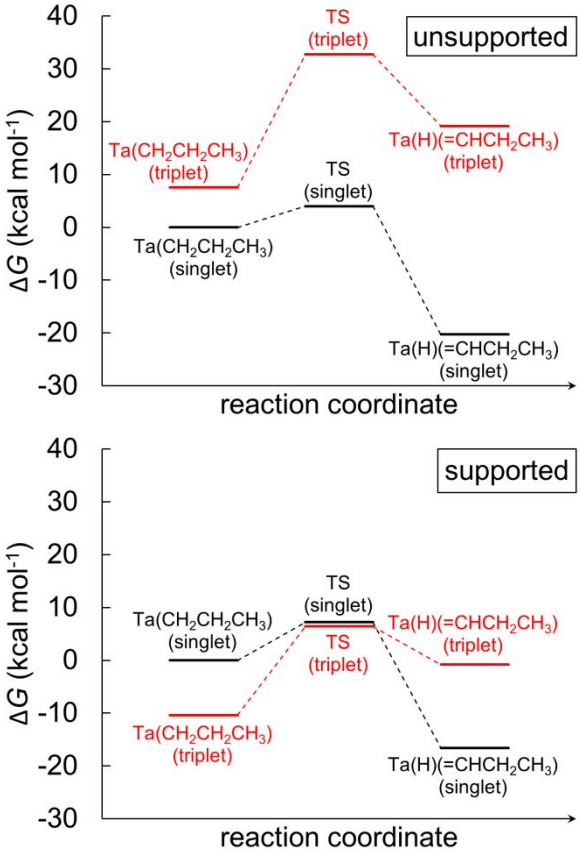

Figure 5. Free energy profiles for α-H elimination over (top) unsupported Ta propyl complexes and (bottom) Y_2O_2 @NU-1000-supported Ta propyl complexes. TS denotes the saddle point geometry that connects the Ta propyl and Ta hydride propylidene complexes along the minimum energy path of each spin configuration. The singlet Ta propyl structure is the zero of energy in both diagrams. Computed free energies of reagents and transition states are provided in Table 1.

Due to this stabilization of the triplet spin configuration in the Y_2O_2@NU-1000 supported system, a singlet-triplet PES crossing is observed for the supported catalyst, where the reactant ($Ta(CH_2CH_2CH_3)$) favors the triplet spin state while the product ($Ta(H)(=CHCH_2CH_3)$) favors the singlet spin state. Since Ta is in the third transition-metal row, the effect of spin-orbit coupling can be strong enough to induce a mixed-spin adiabatic state that allows the system to change spin when the system reaches a configuration where the potential energy of the pure singlet and pure triplet states would be nearly equal.[62] Thus we expect that the α-H elimination over Y_2O_2@NU-1000 supported Ta-based catalyst begins with the energetically more favorable triplet reactant, moves through the triplet transition state with a free energy of activation of

16.4 kcal/mol, followed by the spin crossing region along the reaction pathway, and reaches the singlet product with a free energy of reaction of -6.2 kcal/mol.

Table 1. Calculated free energies (kcal/mol) of singlet and triplet Ta propyl, Ta hydride propylidene, and the corresponding α-H elimination transition state geometries (TS) for the unsupported and Y_2O_2@NU-1000-supported systems. The singlet Ta propyl complex is the reference state in both cases.

	structure	singlet	triplet
unsupported	Ta propyl	0.0	7.5
	TS	4.0	32.7
	Ta hydride propylidene	-20.3	19.2
supported	Ta propyl	0.0	-10.4
	TS	7.2	6.4
	Ta hydride propylidene	-16.6	-0.8

3.1.2 Charge and spin transfer

Charge analyses were carried out for the optimized unsupported and Y_2O_2@NU-1000-supported Ta propyl complexes by the CM5[63] method; the results are summarized in the Appendix as Table A1 and Table A2, respectively. Hirshfeld population analysis[64,65,66] was performed for the same systems to acquire the Hirshfeld spin densities, and the CM5 spin densities are the same as the Hirshfeld spin densities and are reported in Table A1 and Table A2.

Comparing the charges and spin densities between unsupported and Y_2O_2@NU-1000-supported Ta propyl complexes, we observed a charge transfer process that is unique to the supported system. The process, as illustrated in Figure 6, occurs when the spin state of the supported Ta propyl complex changes from singlet to triplet, and involves the Ta ion transfers 0.32 down-spin electrons to the benzoates, at the same time, 0.245 down-spin electrons in the Ta ion populate other *d*-orbitals and flip their spin. This charge transfer process results the Ta ion in the triplet Ta propyl complex to possess only 0.81 spin density with the other 1.19 spin density reside mainly on the benzoates. (The total spin density of a triplet is 2.00.) We find that the ligated Ta ions can have small splittings of their *d*-orbitals and therefore a high spin configuration of the Ta ion is accessible. Also, the calculated SCF molecular orbitals (shown in Appendix

as Figure A1) show that the highest singly occupied molecular orbital (SOMO) and lowest unoccupied molecular orbital (LUMO) of the Y_2O_2@NU-1000 supported Ta propyl complex are the antibonding π-orbitals of the benzoate linkers which proves that some electrons within the benzoate linkers are also in high-lying orbitals and change their spin. This charge transfer process was not observed in the unsupported Ta propyl complex and the Ta ion in the unsupported triplet system possess a total spin density of 1.82. A similar charge transfer behavior can be observed in our calculations in other Y_2O_2@NU-1000 supported complexes including Ta and W-based hydride, hydride propylidene, hydride propyl, hydride with associated propene molecule, and Nb-based propyl complex.

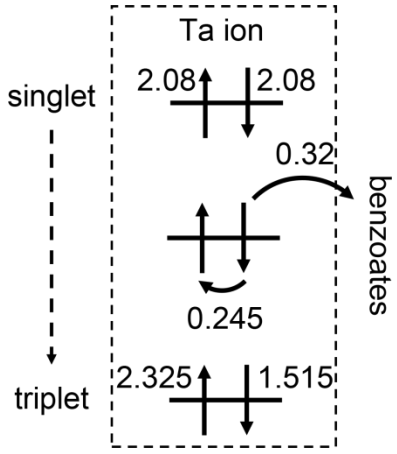

Figure 6. The inter-group and intra-group charge transfer process observed for the Ta ion in the Ta propyl complex supported on Y_2O_2@NU-1000. The ↑ and ↓ arrows denote up-spin electrons and down-spin electrons respectively. Based on the CM5 charge analyses, the Ta ion in the singlet complex has 2.08 up-spin electrons and 2.08 down-spin electrons, and the Ta ion in the triplet complex has 2.325 up-spin electrons and 1.515 down-spin electrons. See Table A2 for the complete data set of CM5 charge and spin density analyses for the Y_2O_2@NU-1000 supported Ta propyl complex.

The observed inter-group (i.e. between the transition-metal and the benzoate linkers) and intra-group (i.e. within the transition-metal and within the benzoates) charge transfer processes are mainly induced by the carboxylate group ($-COO^-$) of the benzoate linkers and the yttria between the transition-metal and the NU-1000 node. Modifying the Y_2O_2@NU-1000 supported Ta propyl complex by replacing benzoates with formates results in the same charge transfer process with the Ta ion losing 0.25

electrons and gaining 0.82 spin densities (based on CM5 charge scheme) when the complex changes from the singlet to triplet.

Tests over W-based propyl complexes reveal that removing yttria and attaching the W atom directly onto the NU-1000 node removes the charge transfer capability of the system. The Ta-based system is not considered for this test because, upon removing the yttria, the Ta atom forms three single bonds with the NU-1000 node and the resulting Ta(III) bare complex cannot perform hydrogen elimination reaction while the W(IV) propyl complex with d^2 W still can. The structures for pristine NU-1000 supported Ta bare complex and W propyl complex are given in Figure 7. For the Y_2O_2@NU-1000 supported W bis(propyl) complex, the CM5 charge difference on W between the singlet and the triplet is 0.19. For the triplet structure, the W ion has spin densities of 0.84. Upon removing yttria, the charge difference of the W ion between singlet and triplet becomes negligible (0.00) and the W ion possesses a spin density of 1.61 in the triplet structure.

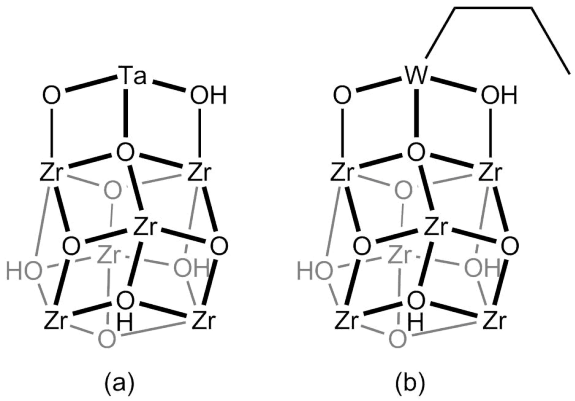

Figure 7. Schematic structures of (a) Ta bare and (b) W bis(propyl) complexes deposited on pristine NU-1000 MOF. Benzoate groups are used to replace the benzoate pyrene linkers of the NU-1000 node but are unshown in the figure for display purposes. Cartesian coordinates for optimized structure (b) are provided in the Online Resource 2. Structure (a) is not optimized.

To test the metal specificity of the effect, we replaced the two Y atoms in the Y_2O_2@NU-1000 with two Al atoms, and we found that the W bis(propyl) complex supported on Al_2O_2@NU-1000 does not show the inter-group and intra-group charge transfer. In other words, replacing the yttria with alumina in the W bis(propyl) complex supported on Y_2O_2@NU-1000 has the same effect on charge transfer as removing Y_2O_2.

The enabling of intra-group and inter-group electron flow by Y_2O_2@NU-1000

support is expected to affect the reaction energetics, and we next consider quantitative estimations of the energetics. Upon comparing the Ta hydride complex to the propyl or other larger functional groups, the hydride (−H) has the least interaction with the Y_2O_2@NU-1000 node, which helps in isolating the energetic effect of the intra-group and inter-group electron transfer. The inter-group and intra-group charge transfers can be observed for the Y_2O_2@NU-1000 supported Ta hydride complex; the charge difference between the singlet and the triplet for the Ta ion is 0.12, and the spin density for Ta ion in the triplet structure is 1.48. The free energy difference between the singlet and triplet structures for the Y_2O_2@NU-1000 supported Ta hydride complex is 0.5 kcal/mol and is very close to that for its unsupported counterpart (-2.0 kcal/mol). In comparison to the Ta hydride system, the free energy difference between the singlet and triplet Ta propyl complexes is -10.4 kcal/mol for the Y_2O_2@NU-1000 supported structures, and is 7.5 kcal/mol for the unsupported structures. One plausible hypothesis for the effect of charge transfer is that it enables certain functional groups, such as propyl, to interact more strongly with the applied support and stabilize the structure.

3.2 Active site effect: Catalyst screening over transition-metal-functionalized, yttria-decorated NU-1000

We considered six transition metals, namely V, Nb, and Ta from group 5 and Cr, Mo, and W from group 6, for catalyzing the hydrogen elimination reaction. Specifically, the reactions considered are:

$$M(Fr)(C_3H_7)_n \rightarrow M(Fr)(H)(=CHCH_2CH_3)(C_3H_7)_{n-1} \quad (R1)$$

$$M(Fr)(C_3H_7)_n \rightarrow M(Fr)(H)(C_3H_7)_{n-1}(CH_2=CHCH_3) \quad (R2)$$

$$M(Fr)(H)(C_3H_7)_{n-1}(CH_2=CHCH_3) \rightarrow M(Fr)(H)(C_3H_7)_{n-1} + C_3H_6 \quad (R3)$$

where M denotes the deposited metal, Fr denotes the Y_2O_2@NU-1000 framework, and n is 1 or 2 (see Figure 2), depending on the initial formal oxidation state considered for each transition metal.

Reaction 1 (R1) is the α-H elimination reaction in which an H atom transfers from the α-C atom of the propyl group to the transition metal and generates a metal hydride propylidene complex. Reaction 2 (R2) is the β-H elimination reaction where an H atom is transferred from the β-C of the propyl group to the transition metal to produce a metal hydride and an adsorbed propene molecule; the propene molecule is released (desorbs) from the metal center in reaction 3 (R3).

Our calculations on the Y_2O_2@NU-1000 supported W system show that the desorption of the propene molecule from the W hydride has no intrinsic barrier (i.e., the reverse association is barrierless). We, therefore, assumed for all the transition metals

that the propene release reaction (R3) has no intrinsic barrier; the free energies of release (ΔG) are used as part of the proposed catalyst screening volcano plot (see below).

For R1 and R2, the V, Nb, Ta, and Cr ions are initially in the +3 oxidation state for the illustrated propyl complex (Figure 2(a)), and the Mo and W ions are initially in the +4 oxidation state for the bis(propyl) complex (Figure 2(b)); the formal oxidation state of the transition-metal increases by 2 during the H elimination reaction when the propyl group transfers an H atom to the metal to form a hydride alkylidene. The oxidation number stays constant when it forms a hydride with an adsorbed propene molecule (although the total electron count increases by 2 since the metal picks up a new π-bound ligand and replaces a propyl ligand with an H ligand). Note, the Cr(III) ion is chosen for our screening study because, among the common oxidation states for Cr ion (including +2, +3, and +6), only the Cr(III) can perform the hydrogen elimination reaction when deposited on Y_2O_2@NU-1000. The Cr(II) ion would bind with the support through 2 Cr–O bonds and give Cr(II) bare complex with no alkyl group available for the hydrogen elimination reaction, and the Cr(VI) ion would have a saturated coordination environment and therefore also cannot perform the hydrogen elimination reaction.

The most energetically stable spin state of the intermediates may change during the reactions. All of the free energies reported in this article are based on the most stable spin state of each case. Details regarding the structures and energies of reagents and transition structures are provided in the Online Resources 1 and 2. Free energy profiles for α-H elimination and β-H elimination over transition-metal functionalized Y_2O_2@NU-1000 catalysts are provided in Figure 8 with the corresponding free energies of activation for the hydrogen elimination reactions and the free energies of release for the propene molecule summarized in Table 2. The correlation between the free energy of activation for α-H elimination and that for β-H elimination is shown in Figure 9.

For the six screened transition-metal catalysts deposited on Y_2O_2@NU-1000, the free energies of activation for α-H elimination (R1) vary between 5.8 and 43.2 kcal/mol. The β-H eliminations (R2) always exhibit lower barriers than the α-H eliminations. This can be rationalized by the H atoms at the β-C position of the propyl group having more structural flexibility than the ones on the α-C and being better aligned for interacting with the empty *d*-orbital of the metal site. The most active catalyst for both α-H elimination and β-H elimination is the Nb-based system, with a $\Delta G^{\ddagger}$ of 5.8 kcal/mol in the former case and 3.2 kcal/mol in the latter. A Bell–Evans–Polanyi (BEP) relationship[67,68,69,70,71,72] is found to hold well for both the α-H and β-H elimination reaction, as shown by the free energy of activation being a linear function of the free energy of reaction in Figure A2 in the Appendix.

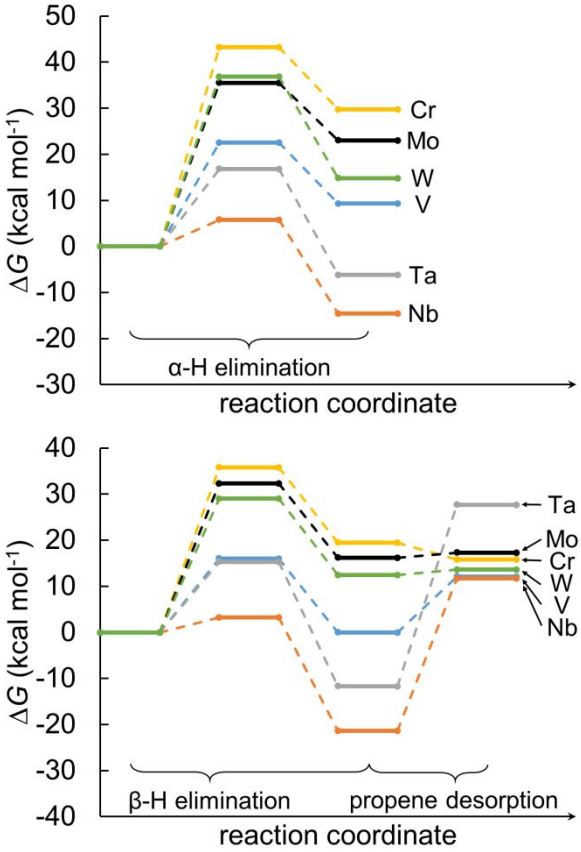

Figure 8. Free energy profiles for (top) α-H elimination and (bottom) β-H elimination with its company propene desorption step over transition-metal functionalized Y_2O_2@NU-1000 catalysts. Computed free energy of activation ($\Delta G^{\ddagger}$, kcal/mol) for the α-H and β-H elimination reactions and free energy of release (ΔG, kcal/mol) for the propene desorption are summarized in Table 2.

Table 2. Computed free energy of activation ($\Delta G^{\ddagger}$, kcal/mol) for the α-H and β-H elimination reactions and free energy of release (ΔG, kcal/mol) for the propene desorption over transition-metal functionalized Y_2O_2@NU-1000 MOFs.

	V	Nb	Ta	Cr	Mo	W
α-H elimination ($\Delta G^{\ddagger}$)	22.5	5.8	16.8	43.2	35.5	36.8
β-H elimination ($\Delta G^{\ddagger}$)	16.0	3.2	15.3	35.8	32.3	29.0
propene desorption (ΔG)	12.1	33.1	38.9	-3.7	1.1	1.2

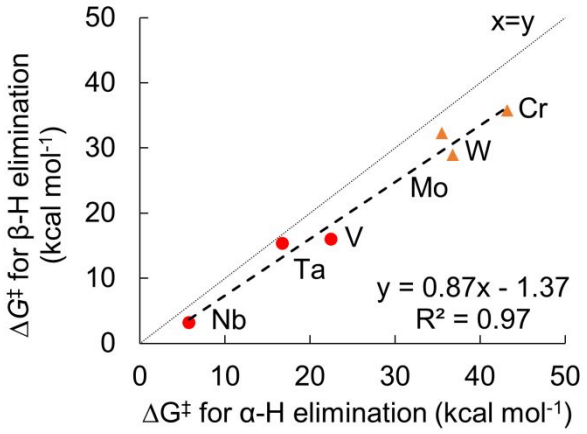

Figure 9. Gibbs free energy of activation for α-H elimination over transition-metal functionalized Y_2O_2@NU-1000 plotted against that for β-H elimination.

The propene molecule produced in the β-H elimination reaction is coordinated to the metal center after the elimination step (R2) and requires energy to desorb. We found that the computed free energy of desorption for the propene molecule is inversely related to the free energy of activation for the β-H elimination reaction. The inverse correlation between the free energy of activation for β-H elimination and the free energy of propene desorption is shown in Figure 10. Because the Nb-based system has a high free energy of propene desorption, in particular 33.1 kcal/mol, it should have poor catalytic performance even though it has the lowest free energy of activation for the β-H elimination step.

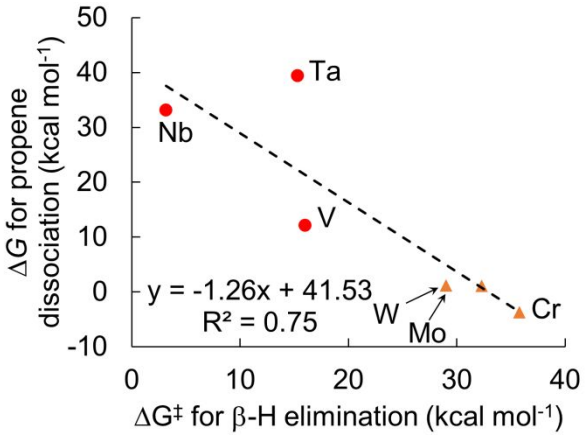

Figure 10. Free energy of activation for β-H elimination over transition-metal functionalized Y_2O_2 @NU-1000 MOFs plotted against free energy of propene desorption from the Y_2O_2 @NU-1000 supported metal hydride complexes.

Note that the Y_2O_2@NU-1000 supported Ta-based system is an outlier in Figure 10 in that the barrier for the hydrogen elimination reaction does not correlate well with the propene desorption energy. It is higher than expected from the correlation, probably because of the existence of a low-lying reactant species (Ta propyl complex) on the triplet PES which is stabilized by the applied Y_2O_2@NU-1000 support, as described in the previous section.

Figure 11 plotted the β-H elimination step and the propene desorption step for six tested Y_2O_2@NU-1000 supported systems. The plot shows, among the six catalytic candidates we have considered, the vanadium-functionalized Y_2O_2@NU-1000 MOF is predicted to be the best catalyst for the β-H elimination reaction. The other transition-metal-based systems are more energetically demanding in terms of either reactant activation or product desorption. Even though V-functionalized, yttria-decorated NU-1000 MOF is yet-to-be-synthesized, yttria has been deposited experimentally on zirconia through the atomic layer deposition method[42,43] and vanadia-functionalized MOF NU-1000 is also experimentally available[73,74].

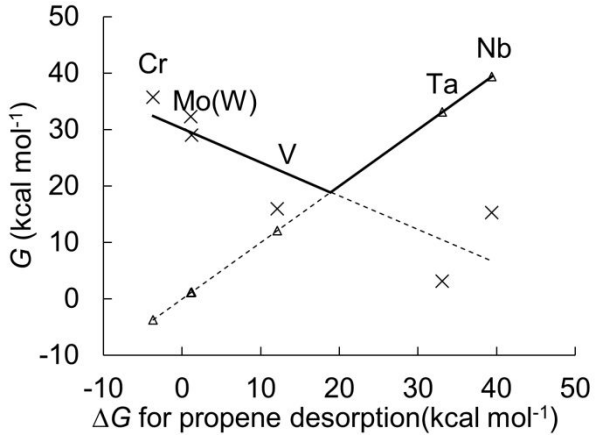

Figure 11. Volcano plot for β-H elimination. For each transition-metal, "×" represents the free energy of activation for β-H elimination over the corresponding transition-metal functionalized Y_2O_2@NU-1000 MOF, and the "Δ" below or above it represents the free energy of desorption of the associated propene.

4. Concluding Remarks

Because of their tunable structures, MOFs offer new opportunities for rational catalyst design based on structure-reactivity relationships. In this article, we used density-functional-based computational simulations to evaluate the use of a yet-to-be-synthesized MOF, in particular, yttria-decorated NU-1000, as a support for the development of new heterogeneous hydrogen elimination catalyst.

We calculated the mechanisms, free energies of reaction, and free energies of activation of hydrogen elimination reactions for the computational screening of six transition-metals: V, Nb, Ta, Cr, Mo, W. Of the six metals studied, we identified the Nb-functionalized, yttria-decorated NU-1000 as the most efficient catalyst for both kinds of hydrogen elimination steps; the associated free energies of activation for α-H and β-H eliminations reactions were calculated to be 5.8 and 3.2 kcal/mol, respectively. Unlike the α-H elimination reaction where a propylidene functional group is produced, the β-H elimination reaction produces an adsorbed propene molecule as one of the products, and we also considered the propene desorption process in our screening study. We constructed a volcano plot using the free energy of activation of the β-H elimination and the free energy of desorption of propene. Based on the Sabatier principle, which states that the optimal catalyst for a given catalytic reaction is the one that interacts with atoms and molecules with intermediate strength for easy reactant activation as well as easy product desorption, we identified V-functionalized, yttria-decorated NU-1000 as the most active catalyst among the trial candidates for the β-H elimination reaction with

the corresponding free energy of activation and propene free energy of desorption calculated to be 16.0 and 12.1 kcal/mol, respectively.

To understand the support effect of Y_2O_2@NU-1000 MOF, charge and spin density analyses were applied to the catalytic intermediates. The analyses reveal a simultaneous inter-group and intra-group charge transfer that occurs in certain Y_2O_2@NU-1000-supported metal complexes when they change their spin configurations. Considering the transition-metal ion and benzoate groups of the Y_2O_2@NU-1000 node as two subsystems, when the total spin multiplicity of the Y_2O_2@NU-1000 supported system changes, an electron flow can be observed between the two subsystems and a portion of the untransferred electron density changes spin within each subsystem, causing each subsystem to exhibit a larger change in spin density than its change in partial charge. Our calculation shows that the inter-group and intra-group charge transfer is mainly induced by the carboxylate groups ($–COO^–$) in the MOF linkers and the yttria between the transition-metal and the Zr_6 node of the NU-1000 MOF. Complexes including, but not limited to, Ta-based and W-based hydride, propyl, and hydride propylidene intermediates and Nb-based propyl intermediates exhibit such charge transfer behavior. Case study of the Ta-based complexes reveals that the effect of the Y_2O_2@NU-1000 support on the Ta catalyst is to stabilize the triplet configuration of the intermediates and consequently increasing the free energy of activation for the H elimination reaction.

5. Electronic Supplementary Material

A table of energies, enthalpies, and free energies of transition-metal-functionalized Y_2O_2@NU-1000 complexes is available in file ESM_1.pdf. Optimized Cartesian coordinates (XYZ) of transition-metal-functionalized Y_2O_2@NU-1000 complexes, W functionalized Y_2O_2@NU-1000 and pristine NU-1000 complexes have been prepared as separate files, which may be opened as text files to read the coordinates or opened directly by a molecular modeling program such as Mercury for visualization and analysis. These text files are gathered into a file called ESM_2.zip.

ACKNOWLEDGMENTS

This work was supported as part of the Inorganometallic Catalyst Design Center, an Energy Frontier Research Center funded by the U.S. Department of Energy, Office of Science, Basic Energy Sciences under award DE-SC0012702.

APPENDIX

A1. Charge and spin density analysis of the Ta propyl complex and the calculated SCF singly occupied molecular orbitals for the Y_2O_2@NU-1000 supported system

Table A1 and Table A2 summarize the computed CM5 charges and spin densities for the optimized unsupported Ta propyl complex and the Y_2O_2@NU-1000-supported Ta propyl complexes.

As shown in A1, for the unsupported singlet Ta propyl complex, the Ta ion has a positive charge of 0.80. The computed charge also shows that a small charge transfer of ~0.1 can be observed between the Ta ion and the propyl group when comparing the triplet to the singlet structure. In the unsupported triplet structure, the electronic spin mostly resides on the Ta ion with a spin density of 1.82, and only 0.18 of the spin density is distributed to the propyl and hydroxyl groups. (The total spin density of a triplet is 2.00.) There is only a small charge difference between the singlet and triplet structures of the Ta ion, and in the triplet the Ta ion holds most of the spin density; this indicates that the spin density on the Ta ion in the triplet structure mainly results from the change of down-spin electrons on the Ta ion in the singlet geometry to up-spin electrons on Ta in the triplet geometry .

Table A1. Computed CM5 charges and spin densities for the optimized unsupported Ta propyl complex (Figure 4, left). Charges and spin densities are tabulated according to the types of atoms and functional groups.

	Ta	**propyl**	**hydroxyl**	
			2O	**2H**
		CM5 charges		
singlet	0.80	-0.20	-1.31	0.71
triplet	0.91	-0.27	-1.33	0.69
Δ*	0.11	-0.07	-0.02	-0.02
		CM5 spin densities		
singlet	0.00	0.00	0.00	0.00
triplet	1.82	0.11	0.05	0.02
Δ*	1.82	0.11	0.05	0.02

*difference in charge or spin density (triplet minus singlet)

However, this is not the case for the complex supported on Y_2O_2@NU-1000. As shown in Table A2, for the supported triplet Ta propyl complex, a spin density of only

0.81 resides on the Ta ion with 0.88 residing on the benzoate linkers of the support. (Two (#3, #4) of the eight linkers possess most of the 0.88 spin density.) For the supported Ta propyl complex, when comparing the triplet to the singlet structure, the charge of the Ta ion increases by 0.32, and the charge of the eight benzoate linkers decreases by 0.42.

Since it is simpler to analyze a single ion than multiple benzoate groups, we use CM5 charges and spin densities of the Ta ion to discuss the charge transfers and spin density changes as shown in Table A2. For the singlet structure, the Ta ion has charge of +0.84 with 2.08 up-spin electrons and 2.08 down-spin electrons. (The neutral Ta has five valence electrons). For the triplet structure, the Ta ion has charge of +1.16 with a spin density of 0.81, hence 2.325 up-spin electrons and 1.515 down-spin electrons. When comparing the triplet structure to the singlet, the Ta ion loses 0.32 electrons net, but it does this by gaining 0.245 up-spin electrons and losing 0.565 down-spin electrons.

Table A2. Computed CM5 charges and spin densities for the optimized Ta propyl complex supported on Y_2O_2@NU-1000 supported (Figure 4, right). Charges and spin densities are tabulated according to the types of atoms and functional groups. Eight benzoate linkers are summarized individually, with the #1, #2, #3, #4 benzoate linkers being the ones that are closer to the Ta ion.

	Ta	**propyl**	**Y_2O_2**		**Zr_6 node**	
			2Y	**2O**	**6Zr**	**16O**
			CM5 charges			
singlet	0.84	-0.25	2.76	-1.51	8.90	-11.47
triplet	1.16	-0.25	2.78	-1.50	8.90	-11.41
Δ*	0.32	0.01	0.02	0.01	-0.01	0.06
			CM5 spin densities			
singlet	0.00	0.00	0.00	0.00	0.00	0.00
triplet	0.81	0.04	0.08	0.03	0.11	0.05
Δ*	0.81	0.04	0.08	0.03	0.11	0.05

benzoate linkers

	#1	**#2**	**#3**	**#4**	**#5**	**#6**	**#7**	**#8**
				CM5 charges				
singlet	-0.37	-0.38	-0.42	-0.41	-0.41	-0.40	-0.40	-0.41
triplet	-0.36	-0.38	-0.65	-0.57	-0.41	-0.43	-0.42	-0.41
Δ*	0.01	0.00	-0.23	-0.16	0.00	-0.02	-0.02	0.00

	CM5 spin densities							
singlet	0.00	0.00	0.00	0.00	0.00	0.00	0.00	0.00
triplet	0.01	0.01	0.47	0.30	0.00	0.05	0.04	0.00
Δ*	0.01	0.01	0.47	0.30	0.00	0.05	0.04	0.00

*difference in charge or spin density, Δ(triplet - singlet)

The uneven distribution of the spin densities over benzoate linkers in the supported Ta propyl system, as observed in Table A2, can be explained as follows. As shown in Figure A1, the supported Ta propyl complex cluster has eight benzoate linkers (four linkers that are directed behind the plane of the page are covered by the four linkers directed toward the front of the plane). The cluster also has two Y atoms on the "top" face of NU-1000 node, and each Y atom is in close proximity to two benzoate linkers. Each of the two linkers on the top right corner of the cluster (#3 and #4 in Table A2) forms a partial bond with the right Y atom through a partial Y–O bond (the O atom in this Y–O bond is the O atom of the corresponding carboxylate group that is close to the right Y atom). The calculated Y–O bond distances are 2.41 Å and 2.42 Å respectively for linker #3 and linker #4 in the geometry-optimized structure. Using the same definitions, the calculated distances of 2.54 Å and 3.39 Å between the left Y atom and the two top left linkers (#1 and #2 in Table A2) are obtained for linker #1 and #2 in the geometry-optimized structure respectively. The partial bonds between the right Y atom and the right linkers provide necessary charge transfer pathway between the Ta atom and the linkers for the charge and spin transfer, as indicated in Figure 6 of the manuscript proper. Comparing to the two Y–O pairs on the right, the longer distances between Y and O atoms of the left two Y–O pairs prevent the charge and spin transfer from occurring, and it is this disparity in distances that causes the observed asymmetric distribution of the spin densities among organic linkers.

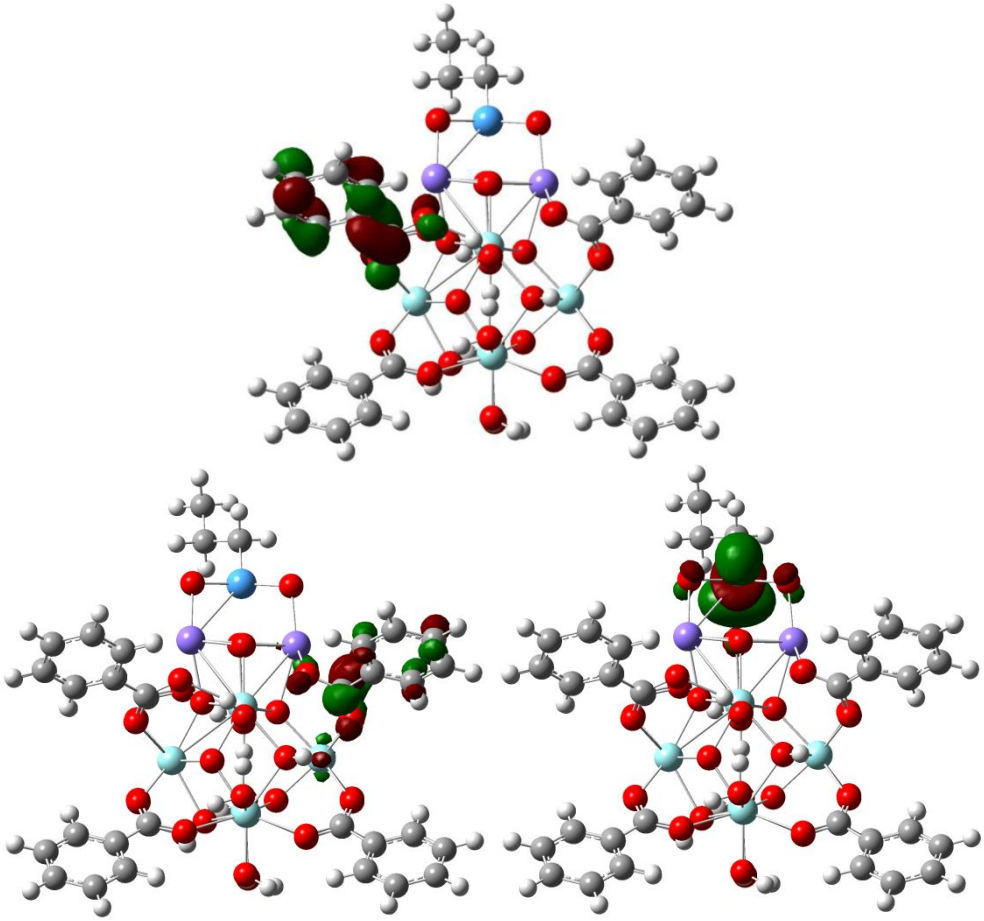

Figure A1. The triplet Ta propyl complex supported on Y_2O_2 @NU-1000 with the LUMO (top part of figure), the highest (bottom left) and the second highest (bottom right) SOMOs shown. (C atoms in grey, H in white, O in red, Zr in cyan, Y in purple, Ta in blue.)

A2. Analyses on the Y_2O_4-supported Ta-based complexes

As mentioned in section 3.1.2 of the main text, the applied yttria layer between the transition-metal complex and the Zr_6 node plays an important role in assisting the observed intra- and inter-group charge transfer. The effect of the yttria layer is isolated and studied in this section using the Y_2O_4-supported model. The model, as shown in Figure A2, was extracted from the optimized Y_2O_2 @NU-1000-supported Ta propyl complex. The Y atoms in the Y_2O_4-supported model have formal oxidation state of +3 which is the same as that for the Y atoms in the Y_2O_2 @NU-1000-supported model. The α-H elimination reaction was then tested over the Y_2O_4-supported Ta(propyl) complex on both singlet and triplet potential energy surfaces. The corresponding free energy profiles are given in Figure A3 with the free energies for singlet and triplet Ta propyl, Ta hydride propylidene, and the corresponding α-H elimination transition state

geometries (TS) provided in Table A3.

Figure A3 may be compared with Figure 5 of the main text which includes the free energy profiles for α-H elimination over unsupported Ta propyl complexes and Y_2O_2@NU-1000-supported Ta propyl complexes. As discussed in the main text, the effect of the Y_2O_2@NU-1000 support is to stabilize the triplet spin configuration of the Ta-based complexes, and – in comparison – Figure A3 shows that the yttria layer by itself provides a support effect in the same direction, but smaller than that of the Y_2O_2@NU-1000 support. As summarized in Table 1 of the article paper and Table A3 below, the triplet Ta propyl complex in the unsupported system favors the singlet spin state over the triplet by a free energy of 7.5 kcal/mol, but the triplet spin state is favored by a free energy of 0.8 kcal/mol in the Y_2O_4-supported system and a free energy of 10.4 kcal/mol in the Y_2O_2@NU-1000-supported system.

The same trend can be observed for the α-H elimination transition state geometry and the Ta hydride propylidene complex, namely that the TS geometry favors the singlet spin state over the triplet by a free energy of 28.7 kcal/mol in the unsupported system, and by a free energy of 9.2 kcal/mol in the Y_2O_4-supported system, but favors the triplet spin state by a free energy of 0.8 kcal/mol in Y_2O_2@NU-1000-supported system. The Ta hydride propylidene favors the singlet spin state by free energies of 39.5, 28.4, and 15.8 kcal/mol respectively in unsupported system, in Y_2O_4-supported system, and in Y_2O_2@NU-1000-supported system.

CM5 charge and spin density analysis has also been conducted for the Y_2O_4-supported Ta propyl complex. The results are summarized in Table A4. Similarly to the Y_2O_2@NU-1000-supported system, delocalization of the spin density is seen in the triplet Ta propyl complex with the Ta atom possessing a spin density of 0.83 and the two Y atoms possessing a total spin density of 1.02. This observation further suggests that the Y atom facilitates the intra- and inter-group charge transfer as discussed in the article proper. In absence of the benzoate linkers of the Zr6 node, as in the Y_2O_4-supported system, this charge transfer occurs between Y atoms and the Ta atom; however, when the benzoate linkers are present, as in the Y_2O_2@NU-1000-supported system, the Y atoms enable the charge transfer and act as a charge transfer bridge between the Ta atom and the benzoate groups.

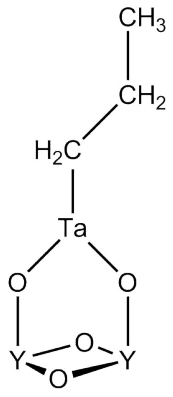

Figure A2. Scheme showing Y_2O_4-supported Ta propyl complex.

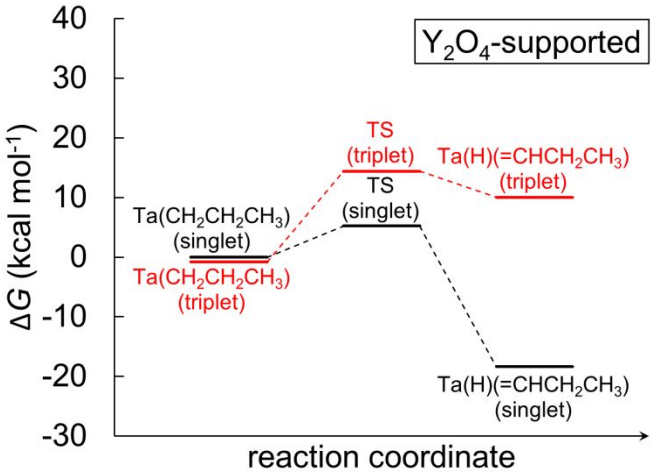

Figure A3. Free energy profiles for α-H elimination over Y_2O_4-supported Ta propyl complexes. TS denotes the saddle point geometry that connects the Ta propyl and Ta hydride propylidene complexes along the minimum energy path of each spin configuration. The singlet Ta propyl structure is the zero of energy. Computed free energies of reagents and transition states are provided in Table A3. All free energies are at a temperature of 298.15 K.

Table A3. Calculated free energies (kcal/mol) of singlet and triplet Ta propyl, Ta hydride propylidene, and the corresponding α-H elimination transition state geometries (TS) for the Y_2O_4-supported systems. The singlet Ta propyl complex is the reference state. All free energies are at a temperature of 298.15 K.

structure	**singlet**	**triplet**
propyl	0.0	-0.8
TS	5.2	14.4
hydride propylidene	-18.4	10.0

Table A4. Computed CM5 charges and spin densities for the optimized Ta propyl complex supported on Y_2O_4. Charges and spin densities are tabulated according to the types of atoms and functional groups.

	Ta	**propyl**	**Y_2O_4**	
			2Y	**4O**
		CM5 charges		
singlet	0.78	-0.26	2.77	-3.29
triplet	1.14	-0.24	2.29	-3.19
Δ*	0.36	0.02	-0.48	0.10
		CM5 spin densities		
singlet	0.00	0.00	0.00	0.00
triplet	0.83	0.05	1.02	0.11
Δ*	0.83	0.05	1.02	0.11

*difference in charge or spin density (triplet minus singlet)

A3. The Bell–Evans–Polanyi (BEP) relationship for α- and β-H elimination reactions

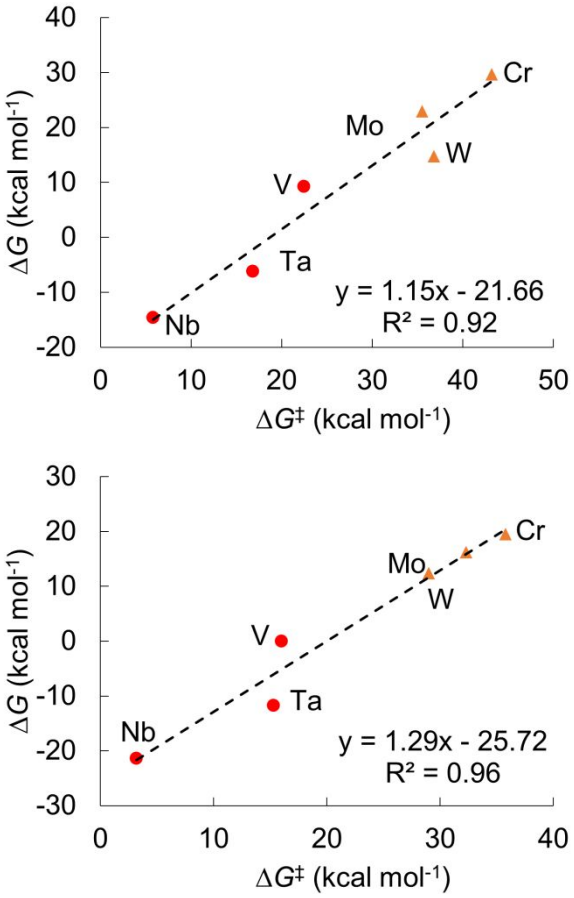

Figure A4. Bell–Evans–Polanyi (BEP) relationship for: (top) α-H elimination reaction, and (bottom) β-H elimination reaction over transition metal functionalized Y_2O_2@NU-1000 MOFs. All free energies are at a temperature of 298.15 K.

REFERENCES

[1] R. H. Crabtree, in *The Organometallic Chemistry of the Transition-metals, 6th ed.*, ed. R. H. Crabtree, John Wiley & Sons, Inc.; Hoboken, New Jersey, 2014, ch. 7, pp. 185–203.

[2] R. J. Cross, in *The Metal – Carbon Bond: Volume 2*, ed. F. R. Hartley and S. Patai, John Wiley & Sons Ltd.; Chichester, New York, 1985, ch. 8, pp. 559–624.

[3] H. D. Kaesz and R. B. Saillant, *Chem. Rev.*, 1972, **72**, 231–281.

[4] J. D. A. Pelletier and J.-M. Basset, *Acc. Chem. Res.*, 2016, **49**, 664–677.

[5] M. K. Samantaray, E. Pump, A. Bendjeriou-Sedjerari, V. D'Elia, J. D. A. Pelletier, M. Guidotti, R. Psaro and J.-M. Basset, *Chem. Soc. Rev.*, 2018, **47**, 8403–8437.

[6] M. R. Churchill, H. J. Wasserman, H. W. Turner and R. R. Schrock, *J. Am. Chem. Soc.*, 1982, **104**, 1710–1716.

[7] R. H. Crabtree, M. F. Mellea, J. M. Mihelcic and J. M. Quirk, *J. Am. Chem. Soc.*, 1982, **104**, 107–113.

[8] H. Felkin, T. Fillebeen-Khan, Y. Gault, R. Holmes-Smith and J. Zakrzewski, *Tetrahedron Lett.*, 1984, **25**, 1279–1282.

[9] F. Liu, E. B. Pak, B. Singh, C. M. Jensen and A. S. Goldman, *J. Am. Chem. Soc.*, 1999, **121**, 4086–4087.

[10] G. T. Crisp, *Chem. Soc. Rev.*, 1998, **27**, 427–436.

[11] H. Wakamatsu, M. Nishida, N. Adachi and M. Mori, *J. Org. Chem.*, 2000, **65**, 3966–3970.

[12] B. M. Trost and M. J. Krische, *Synlett*, 1998, **1998**, 1–16.

[13] L. A. Van Der Veen, P. C. J. Kamer and P. W. N. M. Van Leeuwen, *Angew. Chem. Int. Ed.*, 1999, **38**, 336–338.

[14] B. Breit, R. Winde and K. Harms, *J. Chem. Soc., Perkin Trans. 1*, 1997, **4**, 2681–2682.

[15] J. D. Fellmann, R. R. Schrock, and D. D. Traficante, *Organometallics*, 1982, **1**, 481–484.

[16] B. M. M. Wheatley and B. A. Keay, *J. Org. Chem.*, 2007, **72**, 7253–7259.

[17] K. Umezawa-Vizzini and T. R. Lee, *Organometallics*, 2004, **23**, 1448–1452.

[18] N. M. Doherty and J. E. Bercaw, *J. Am. Chem. Soc.*, 1985, **107**, 2670–2682.

[19] A. H. Chughtai, N. Ahmad, H. A. Younus, A. Laypkov and F. Verpoort, *Chem. Soc. Rev.*, 2015, **44**, 6804–6849.

[20] J. Liu, L. Chen, H. Cui, J. Zhang, L. Zhang and C. Y. Su, *Chem. Soc. Rev.*, 2014, **43**, 6011–6061.

[21] O. K. Farha, I. Eryazici, N. C. Jeong, B. G. Hauser, C. E. Wilmer, A. A. Sarjeant, R. Q. Snurr, S. T. Nguyen, A. Ö. Yazaydin and J. T. Hupp, *J. Am. Chem. Soc.*, 2012, **134**, 15016–15021.

[22] O. K. Farha, C. E. Wilmer, I. Eryazici, B. G. Hauser, P. A. Parilla, K. O'Neill, A. A. Sarjeant, S. T. Nguyen, R. Q. Snurr and J. T. Hupp, *J. Am. Chem. Soc.*, 2012, **134**, 9860–9863.

[23] H. Furukawa, K. E. Cordova, M. O'Keeffe and O. M. Yaghi, *Science*, 2010, **9**, 1230444.

[24] J. Lee, O. K. Farha, J. Roberts, K. A. Scheidt, S. T. Nguyen and J. T. Hupp, *Chem. Soc. Rev.*, 2009, **38**, 1450–1459.

[25] D. Yang, S. O. Odoh, J. Borycz, T. C. Wang, O. K. Farha, J. T. Hupp, C. J. Cramer, L. Gagliardi and B. C. Gates, *ACS Catal.*, 2016, **6**, 235–247.

[26] C. Copéret, M. Chabanas, R. P. Saint-Arroman and J.-M. Basset, *Angew. Chem. Int. Ed.*, 2003, **42**, 156–181.

[27] C. Copéret, A. Comas-Vives, M. P. Conley, D. P. Estes, A. Fedorov, V. Mougel, H. Nagae, F. Núñez-Zarur, P. A. Zhizhko, C. Copéret, A. Comas-Vives, M. P. Conley, D. P. Estes, A. Fedorov, V. Mougel, H. Nagae, F. Núnez-Zarur and P. A. Zhizhko, *Chem. Rev.*, 2016, **116**, 323–421.

[28] F. Rascon, R. Wischert and C. Copéret, *Chem. Sci.*, 2011, **2**, 1449–1456.

[29] M. M. Stalzer, M. Delferro and T. J. Marks, *Catal. Lett.*, 2015, **145**, 3–14.

[30] M. Tada and Y. Iwasawa, *Coord. Chem. Rev.*, 2007, **251**, 2702–2716.

[31] J. Guzman and B. C. Gates, *Dalton Trans.*, 2003, **2003**, 3303–3318.

[32] B. Rhers, A. Salameh, A. Baudouin, E. A. Quadrelli, M. Taoufik, C. Copéret, F. Lefebvre, J. M. Basset, X. Solans-Monfort, O. Eisenstein, W. W. Lukens, L. P. H. Lopez, A. Sinha and R. R. Schrock, *Organometallics*, 2006, **25**, 3554–3557.

[33] F. Blanc, J.-M. Basset, C. Copéret, A. Sinha, Z. J. Tonzetich, R. R. Schrock, X. Solans-Monfort, E. Clot, O. Eisenstein, A. Lesage and L. Emsley, *J. Am. Chem. Soc.*, 2008, **130**, 5886–5900.

[34] M. P. Conley, V. Mougel, D. V. Peryshkov, W. P. Forrest, D. Gajan, A. Lesage, L. Emsley, C. Copéret and R. R. Schrock, *J. Am. Chem. Soc.*, 2013, **135**, 19068–19070.

[35] A. Salameh, J. Joubert, A. Baudouin, W. Lukens, F. Delbecq, P. Sautet, J.-M. Basset and C. Copéret, *Angew. Chem. Int. Ed.*, 2007, **46**, 3870–3873.

[36] V. Bernales, M. A. Ortuño, D. G. Truhlar, C. J. Cramer and L. Gagliardi, *ACS Cent. Sci.*, 2018, **4**, 5–19.

[37] J. E. Mondloch, W. Bury, D. Fairen-Jimenez, S. Kwon, E. J. Demarco, M. H. Weston, A. A. Sarjeant, S. T. Nguyen, P. C. Stair, R. Q. Snurr, O. K. Farha and J. T. Hupp, *J. Am. Chem. Soc.*, 2013, **135**, 10294–10297.

[38] A. J. Howarth, Y. Liu, P. Li, Z. Li, T. C. Wang, J. T. Hupp and O. K. Farha, *Nat. Rev. Mater.*, 2016, **1**, 15018.

[39] Z. Li, A. W. Peters, V. Bernales, M. A. Ortuño, N. M. Schweitzer, M. R. DeStefano, L. C. Gallington, A. E. Platero-Prats, K. W. Chapman, C. J. Cramer, L. Gagliardi, J. T. Hupp and O. K. Farha, *ACS Cent. Sci.*, 2016, **3**, 31–38.

[40] Z. Li, N. M. Schweitzer, A. B. League, V. Bernales, A. W. Peters, A. B. Getsoian, T. C. Wang, J. T. Miller, A. Vjunov, J. L. Fulton, J. A. Lercher, C. J. Cramer, L. Gagliardi, J. T. Hupp and O. K. Farha, *J. Am. Chem. Soc.*, 2016, **138**, 1977–1982.

[41] M. Rimoldi, V. Bernales, J. Borycz, A. Vjunov, L. C. Gallington, A. E. Platero-Prats, I. S. Kim, J. L. Fulton, A. B. F. Martinson, J. A. Lercher, K. W. Chapman, C. J. Cramer, L. Gagliardi, J. T. Hupp and O. K. Farha, *Chem. Mater.*, 2017, **29**, 1058–1068.

[42] J. H. Shim, C.-C. Chao, H. Huang and F. B. Prinz, *Chem. Mater.*, 2007, **19**, 3850–3854.

[43] C.-C. Chao, Y. B. Kim and F. B. Prinz, *Nano Lett.*, 2009, **9**, 3626–3628.

[44] J. K. Nørskov, T. Bligaard, B. Hvolbaek, F. Abild-Pedersen, I. Chorkendorff and C. H. Christensen, *Chem. Soc. Rev.*, 2008, **37**, 2163–2171.

[45] B. Yang, R. Burch, C. Hardacre, G. Headdock and P. Hu, *ACS Catal.*, 2014, **4**, 182–186.

[46] M. J. Frisch, G. W. Trucks, H. B. Schlegel, G. E. Scuseria, M. A. Robb, J. R. Cheeseman, G. Scalmani, V. Barone, B. Mennucci, G. A. Petersson, H. Nakatsuji, M. Caricato, X. Li, H. P. Hratchian, A. F. Izmaylov, J. Bloino, G. Zheng, J. L. Sonnenberg, M. Hada, K. Ehara, R. Toyota, J. Fukuda, M. Hasegawa, T. Ishida, Y. Nakajima, O. Honda, H. Kitao, T. Nakai, J. A. J. Vreven, J. E. Montgomery, F. Peralta, M. Ogliaro, J. J. Bearpark, E. Heyd, K. N. Brothers, V. N. Kudin, T. Staroverov, R. Keith, J. Kobayashi, J. Normand, K. Raghavachari, A. Rendell, J. C. Burant, S. S. Iyengar, J. Tomasi, M. Cossi, N. Rega, J. M. Millam, M. Klene, J. E. Knox, J. B. Cross, V. Bakken, C. Adamo, J. Jaramillo, R. Gomperts, R. E. Stratmann, O. Yazyev, A. J. Austin, R. Cammi, C. Pomell, J. Cioslowski and D. J. Fox, *Gaussian 09* (Revision E.01), Gaussian, Inc., Wallingford, CT, 2010.

[47] M. J. Frisch, G. W. Trucks, H. B. Schlegel, G. E. Scuseria, M. A. Robb, J. R. Cheeseman, G. Scalmani, V. Barone, G. A. Petersson, H. Nakatsuji, X. Li, M. Caricato, A. V. Marenich, J. Bloino, B. G. Janesko, R. Gomperts, B. Mennucci, H. P. Hratchian, J. V. Ortiz, A. F. Izmaylov, J. L. Sonnenberg, D. Williams-Young, F. Ding, F. Lipparini, F. Egidi, J. Goings, B. Peng, A. Petrone, T. Henderson, D. Ranasinghe, V. G. Zakrzewski, J. Gao, N. Rega, G. Zheng, W. Liang, M. Hada, M. Ehara, K. Toyota, R. Fukuda, J. Hasegawa, M. Ishida, T. Nakajima, Y. Honda, O. Kitao, H.

Nakai, T. Vreven, K. Throssell, J. A. M. Jr., J. E. Peralta, F. Ogliaro, M. J. Bearpark, J. J. Heyd, E. N. Brothers, K. N. Kudin, V. N. Staroverov, T. A. Keith, R. Kobayashi, J. Normand, K. Raghavachari, A. P. Rendell, J. C. Burant, S. S. Iyengar, J. Tomasi, M. Cossi, J. M. Millam, M. Klene, C. Adamo, R. Cammi, J. W. Ochterski, R. L. Martin, K. Morokuma, O. Farkas, J. B. Foresman and D. J. Fox, *Gaussian 16* (Revision A.03), Gaussian, Inc., Wallingford, CT, 2016.

[48] N. Planas, J. E. Mondloch, S. Tussupbayev, J. Borycz, L. Gagliardi, J. T. Hupp, O. K. Farha and C. J. Cramer, *J. Phys. Chem. Lett.*, 2014, **5**, 3716–3723.

[49] D. Yang, S. O. Odoh, T. C. Wang, O. K. Farha, J. T. Hupp, C. J. Cramer, L. Gagliardi and B. C. Gate, *J. Am. Chem. Soc.*, 2015, **137**, 7391–7396.

[50] P. C. Hariharan and J. A. Pople, *Theor. Chim. Acta*, 1973, **28**, 213–222.

[51] M. M. Francl, W. J. Pietro, W. J. Hehre, J. S. Binkley, M. S. Gordon, D. J. DeFrees and J. A. Pople, *J. Chem. Phys.*, 1982, **77**, 3654–3665.

[52] F. Weigend, *Phys. Chem. Chem. Phys.*, 2006, **8**, 1057–1065.

[53] F. Weigend and R. Ahlrichs, *Phys. Chem. Chem. Phys.*, 2005, **7**, 3297–3305.

[54] Y. Zhao and D. G. Truhlar, *J. Chem. Phys.*, 2006, **125**, 194101.

[55] C. J. Cramer and D. G. Truhlar, *Phys. Chem. Chem. Phys.*, 2009, **11**, 10757–10816.

[56] H. S. Yu, X. He and D. G. Truhlar, *J. Chem. Theory Comput.*, 2016, **12**, 1280–1293.

[57] E. I. Ioannidis and H. J. Kulik, *J. Chem. Phys.*, 2015, **143**, 034104.

[58] B. Yang and D. G. Truhlar, *Organometallics*, 2018, **37**, 3917–3927.

[59] Y. Zhao and D. G. Truhlar, *Theor. Chem. Acc.*, 2008, **120**, 215–241.

[60] I. M. Alecu, unpublished, 2011.

[61] L. M. Pratt, D. G. Truhlar, C. J. Cramer, S. R. Kass, J. D. Thompson and J. D. Xidos, *J. Org. Chem.*, 2007, **72**, 2962–2966.

[62] B. Yang, L. Gagliardi, and D. G. Truhlar, *Phys. Chem. Chem. Phys.*, 2018, **20**, 4129–4136.

[63] A. V. Marenich, S. V. Jerome, C. J. Cramer and D. G. Truhlar, *J. Chem. Theory Comput.*, 2012, **8**, 527–541.

[64] F. L. Hirshfeld, *Theoret. Chim. Acta*, 1977, **44**, 129–138.

[65] J. P. Ritchie, *J. Am. Chem. Soc.*, 1985, **107**, 1829–1837.

[66] J. P. Ritchie and S. M. Bachrach, *J. Comp. Chem.*, 1987, **8**, 499–509.

[67] R. P. Bell, *Proc. Royal Soc. Lond. A*, 1936, **154**, 414–429.

[68] J. N. Brønsted, *Chem. Rev.*, 1928, **5**, 231–338.

[69] M. G. Evans and M. Polanyi, *Trans. Faraday Soc.*, 1938, **34**, 11–24.

[70] N. N. Semenov, *Some Problems in Chemical Kinetics and Reactivity*, Princeton University Press; Princeton, New Jersey, 1958.

[71] J. W. Moore and R. G. Pearson, in *Kinetica and Mechanism*, *3rd ed.*, ed. J. W. Moore and R. G. Pearson, John Wiley & Sons, Inc.; New York, 1981, ch. 9, pp. 334–389.

[72] R. A. van Santen, M. Neurock and S. G. Shetty, *Chem. Rev.*, 2010, **110**, 2005–2048.

[73] Y. Cui, M. Rimoldi, A. E. Platero-Prats, K. W. Chapman, J. T. Hupp and O. K. Farha, *ChemCatChem*, 2018, **10**, 1772–1777.

[74] K. Otake, Y. Cui, C. T. Buru, Z. Li, J. T. Hupp and O. K. Farha, *J. Am. Chem. Soc.*, 2018, **140**, 8652–8656.